Journal of The Physical Society of Japan
Vol. 60, No. 11, November, 1991, pp. 3829–3836

Electric Quadrupole Interactions and Magnetic Susceptibility of Icosahedral $Al_{70}Fe_{20}Ta_{10}$

Z. M. STADNIK, G. STROINK,† G. LAMARCHE and A. INOUE††

Ottawa-Carleton Institute for Physics, Department of Physics, University of Ottawa, Ottawa, Ontario K1N 6N5, Canada
†Department of Physics, Dalhousie University, Halifax, Nova Scotia B3H 3J5, Canada
††Institute for Materials Research, Tohoku University, Sendai 980

(Received June 6, 1991)

X-ray diffraction, ^{57}Fe Mössbauer spectroscopy, and magnetic susceptibility measurements have been performed in the temperature range 4.2–293 K on the $Al_{70}Fe_{20}Ta_{10}$ icosahedral alloy. It was found that Fe atoms are distributed among a multiplicity of sites, which was interpreted as evidence of intrinsic disorder characteristic for icosahedral alloys. It was shown that the distribution of electric quadrupole interactions is better described by the Gaussian shape than by the shape predicted by the shell model. It was found that $Al_{70}Fe_{20}Ta_{10}$ is not magnetically ordered. We find that $Al_{70}Fe_{20}Ta_{10}$ is a paramagnet and that the claim made in the literature of the simultaneous occurrence of Curie-like and Pauli paramagnetism is an artifact resulting from previously unconsidered second phases.

§1. Introduction

Since the important discovery of an icosahedral phase in Al–Mn alloys by Shechtman *et al.*,[1] many other icosahedral alloys (IA) have been found,[2] and many are yet to be discovered.[3] It is remarkable that the majority of IA are Al based, i.e., they usually contain a much larger at. % of Al than that of other elements. The main thrust of research has been directed at elucidating their complex atomic structure. Although significant progress has been made in this respect in the last few years,[4] it is still not clear which of the three competing structural models (icosahedral quasicrystal model,[5] icosahedral glass model,[6] and random-tiling model[7]) is the best description of the atomic structure of IA. Furthermore, within a given structural model, the problem of the exact positions of atoms remains unsolved. Such experimental techniques as Mössbauer spectroscopy (MS) or NMR, which are sensitive to local physical properties, are useful in shedding some light on the local atomic structure of IA.[8,9]

As the quality of the samples of IA steadily improved, various experimental techniques began to be applied to study the physical properties of these interesting alloys. However, many of the IA cannot be produced at present as 100% single phase, and typically a few percent of a crystalline second phase, or phases, are present in many IA. While such a small amount of impurity has only a negligible effect on many physical parameters studied, it may significantly alter other parameters which are very sensitive to impurities. This is especially true in studies of magnetic properties of IA, as has been recently demonstrated by Stadnik and Stroink.[10] Caution should be therefore exercised in reporting any "unusual" experimental behaviour of physical properties of IA since they may originate not from the icosahedral structure but from the presence of second phases in the studied IA.

A new ternary icosahedral alloy, $Al_{70}Fe_{20}Ta_{10}$, has been recently produced by rapid solidification by Tsai *et al.*[11] This alloy has a high concentration of Fe, which might make it magnetically ordered, and a relatively high thermal stability. Its magnetic susceptibility, χ, measured in an external magnetic field of 10 kOe was reported[12] to have an unusual temperature dependence, which was inter-

preted as being due to a combination of Pauli and Curie paramagnetism. This is rather interesting since, with the exception of $Al_{65}Fe_{15}Cu_{20}$ which is a diamagnet,[13,14] the IA which are not magnetically ordered which have been studied so far exhibit the Curie-like $\chi(T)$ dependence characteristic of a paramagnet.

One of the goals of this study is to clarify the problem of the magnetic properties of the $Al_{70}Fe_{20}Ta_{10}$ icosahedral alloy. To achieve this, ^{57}Fe MS and magnetic susceptibility measurements are carried out between 4.2 and 293 K. Furthermore, a detailed comparison between analyses of ^{57}Fe Mössbauer spectra based on the widely used shell model and the novel model recently proposed by Rancourt and Ping[15] is carried out.

§2. Experimental Methods

Two batches of $Al_{70}Fe_{20}Ta_{10}$ icosahedral alloy, referred to below as sample 1 and sample 2, were prepared by rapid solidification. The procedure for the sample preparation has been described elsewhere.[11] The icosahedral structure of the samples was confirmed with X-ray diffraction (XRD) measurements.

^{57}Fe MS measurements were performed at room temperature and at 4.2 K using a Wissel II Mössbauer spectrometer operating in a sine mode. The spectrometer was calibrated with a 6.35-μm Fe foil,[16] which corresponds to the surface density of 0.107 mg ^{57}Fe/cm^2, and the spectra were folded. The surface densities of the samples 1 and 2 were respectively 0.166 and 0.073 mg ^{57}Fe/cm^2. A room-temperature ^{57}Co(Rh) was used for both samples.

Magnetic susceptibility measurements were performed in the temperature range 4.2–270 K using a SQUID magnetometer.[17] The samples were first zero-field cooled and then measured in a constant magnetic field of 25.5 Oe.

§3. Results and Discussion

3.1 *X-ray diffraction data*

The $Al_{70}Fe_{20}Ta_{10}$ icosahedral alloy, contrary to the claim in the literature,[12] cannot be produced using a melt-spinning technique as 100% single phase. The XRD spectrum of sample 1 was practically the same as that shown in Fig. 1(a) in ref. 11. Apart from the lines due to the icosahedral structure, the XRD spectrum of sample 1 contained weak lines originating from the crystalline alloys Al_3Ta and Al_3Fe. The two strongest icosahedral lines [Fig. 1(a) in ref. 11], as opposed to the corresponding lines of almost ideally single phase icosahedral $Al_{65}Fe_{15}Cu_{20}$,[9,18] were located on a rounded maximum, which must be due to the presence of overlapping lines of other minor second phases, as discussed in ref. 10. Sample 2 contained even more second phases and was purposely chosen for the measurements to investigate the influence of larger amount of second phases on Mössbauer and susceptibility parameters. The quasilattice constant[19] a_R was calculated from the formula $13.308/Q(100000)$, where $Q(100000)$ is the scattering wave vector corresponding to the (100000) icosahedral line. The values of a_R are 4.597 and 4.591 Å for samples 1 and 2, respectively. The former value coincides with the value reported by Srinivas *et al.*[12] and is close to the value of 4.579 Å reported by Tsai *et al.*[11] Varying quenching rate parameters did not eliminate the presence of a small amount of second phases. We thus conclude that the second phases, mainly in the form of Al_3Ta and Al_3Fe, are present in the $Al_{70}Fe_{20}Ta_{10}$ samples we analyzed.

3.2 *Mössbauer data*

The ^{57}Fe Mössbauer spectrum of sample 1 at room temperature (Fig. 1) exhibits two broad lines resulting from the electric quadrupole interaction. The full linewidths at half maximum, Γ, obtained from a two Lorentzian fit of the spectrum are 0.426(1) and 0.379(3) mm/s, respectively, for the low velocity and the high velocity lines. This should be compared with the linewidth of 0.240(5) mm/s obtained from the fit of the two inner lines of the Fe calibration foil. Such a large broadening of Γ is clear evidence for the existence of a distribution $P(\Delta)$ of the quadrupole splittings $\Delta=\frac{1}{2}eV_{zz}Q(1+\eta^2/3)^{1/2}$, where V_{zz} is the principal component of the electric field gradient (EFG) tensor, Q is the electric quadrupole moment of the 14.4 keV level of ^{57}Fe, and η is the asymmetry parameter.[20] Consequently, any meaningful analysis has to take this distribution into account. The conventional technique

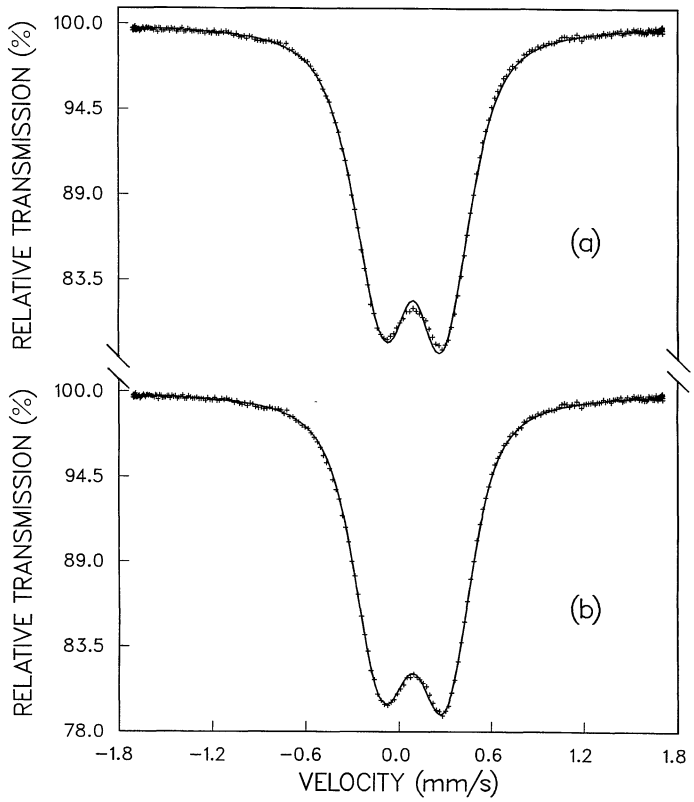

Fig. 1. ^{57}Fe Mössbauer spectrum of sample 1 at 293 K fitted (solid line) with the shell model (a) and with the one-Gaussian-component model (b). The velocity scale is relative to the ^{57}Co(Rh) source.

for analyzing paramagnetic Mössbauer spectra of IA which is based on the fits with a single doublet or with two doublets is methodologically incorrect, as has been discussed in detail elsewhere.[9]

Extraction of the true distribution $P(\Delta)$ from the Mössbauer spectra of disordered alloys, such as amorphous or icosahedral alloys, is not a trivial task. Essentially two general approaches are employed (for a review of various approaches, see refs. 15 and 21). In the first approach, $P(\Delta)$ is expressed in terms of analytical functions based either on an educated guess (for example, a Gaussian function[22]) or on a particular local atomic structure model of a given disordered system (for example, the shell model for amorphous alloys based on random atomic packing[23]). In the second approach, $P(\Delta)$ is expanded in a series of trigonometric or δ-functions with additional constraints.[21] The main advantage of the second approach is its model independence, i.e., it can in principle yield the $P(\Delta)$ distribution which is very close to the true one. However, despite the mathematical effort, the second approach often introduces unrealistic oscillations, especially for spectra of poor statistical quality[24] or for incorrectly chosen fitting parameters. Recently, a new powerful method for obtaining arbitrary-shape static hyperfine parameter distributions from Mössbauer spectra was introduced by Rancourt and Ping.[15] It is based upon representing the true distribution as a sum of Gaussian components and the corresponding spectra are sums of Voight lines. In practice, only very few such components are needed to obtain convergence to a unique distribution.[25] Here we compare the $P(\Delta)$ distributions derived from the fits of the Mössbauer spectra of $Al_{70}Fe_{20}Ta_{10}$ using the shell model[23] and the multi-Gaussian-component model.[15]

In the shell model the distribution function $P(\Delta)=(\Delta^{n-1}/\sigma^n)\exp(-\Delta^2/2\sigma^2)$ is determined by only two parameters: n and σ. The asymmetry of the Mössbauer spectrum (Fig. 1) is taken into account by assuming a linear coupling $\delta=\delta_0+a\Delta$ between the isomer shift, δ, and Δ, where δ_0 and a are the fitted parameters. The fit to the shell model of the room-temperature spectrum of sample 1 is shown in Fig. 1(a) and the corresponding parameters are given in Table I. In the multi-Gaussian-component fit the same linear relation between δ and Δ was used. It turned out that quasi-ideal fits ($\chi^2\sim 1$) could be obtained with only one Gaussian component $P(\Delta)=(1/\sqrt{2\pi\sigma_\Delta})\exp[-(\Delta-\bar{\Delta})^2/2\sigma_\Delta^2]$. The inclusion of the second Gaussian component did not lead to a statistically significant improvement of the fit. The fit to a one-Gaussian-component model of the room-temperature spectrum of sample 1 is shown in Fig. 1(b) and the corresponding parameters are given in Table II. The distributions $P(\Delta)$ obtained from the

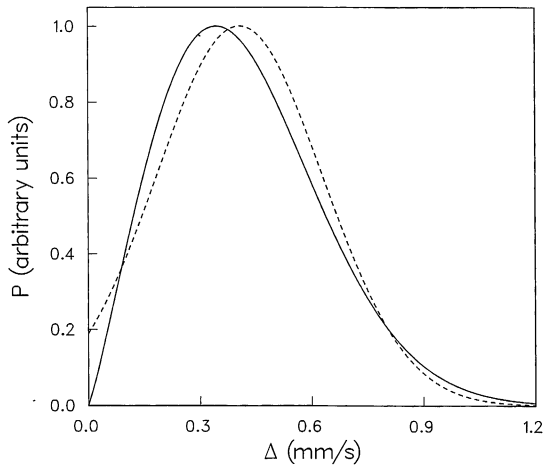

Fig. 2. The distribution function $P(\Delta)$ corresponding to the fits in Figs. 1(a) (solid line) and 1(b) (broken line).

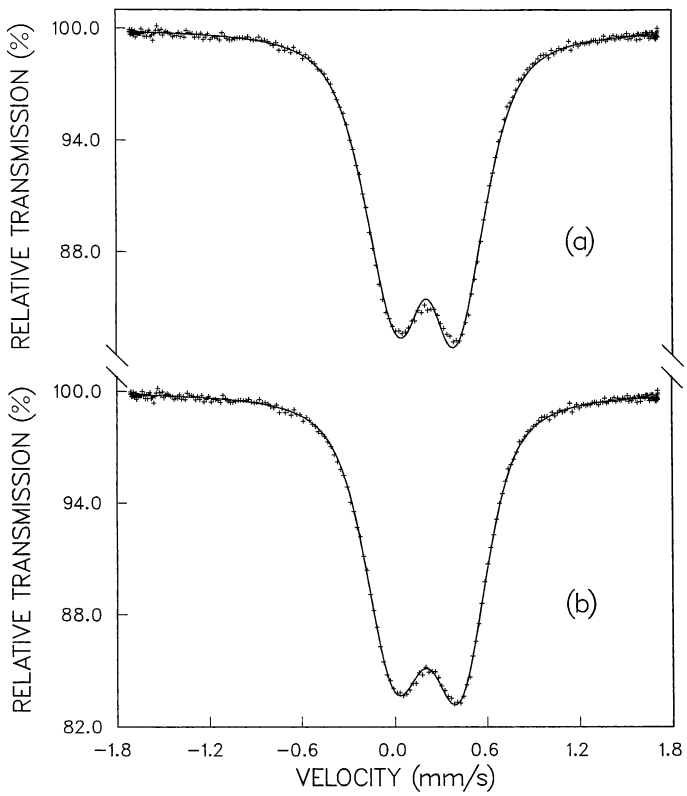

Fig. 3. ^{57}Fe Mössbauer spectrum of sample 1 at 4.2 K fitted (solid line) with the shell model (a) and with the one-Gaussian-component model (b). The velocity scale is relative to the ^{57}Co(Rh) source.

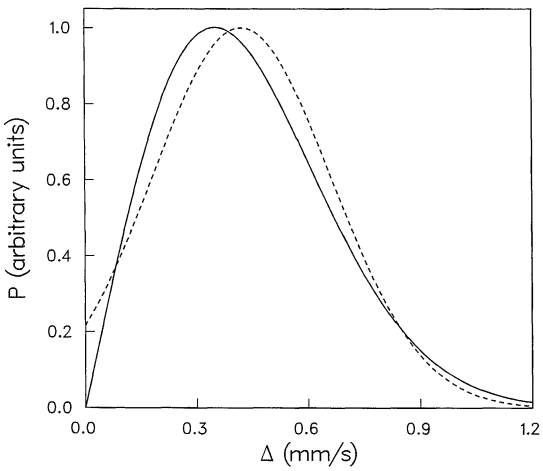

Fig. 4. The distribution function $P(\Delta)$ corresponding to the fits in Figs. 3(a) (solid line) and 3(b) (broken line).

shell-model and one-Gaussian-component-model fits of the room-temperature spectrum of sample 1 are shown in Fig. 2.

The 4.2 K Mössbauer spectrum of sample 1 was analyzed in the same way as the room-temperature spectrum. The fits and the corresponding distributions are shown respectively in Figs. 3 and 4, and the fitted parameters are given in Tables I and II.

It is evident from Figs. 1 and 3 that the one-Gaussian-component-model fits are superior to the shell-model fits. This is also reflected in the values of χ^2 (Tables I and II). In addition to the misfit in the central part of the spectra, the shell model does not give a good fit to the right wing of the spectra [Figs. 1(a) and 3(a)]. The one-Gaussian-component-model, on the other hand, gives almost a perfect fit [Figs. 1(b) and 3(b), and Tables I and II]. The slight misfit in the central part of the spectra [Figs. 1(b) and 3(b)] is evidence for the existence of a small fraction of Al_3Fe (ref. 26) and possibly other Fe-containing second phases.

The values of Γ obtained from the fits (Tables I and II) are now very close to the value of 0.240 mm/s characteristic of the spectrometer and expected for the thicknesses of the absorbers used. This is additional evidence for the validity of fitting the spectra with a distribution of quadrupole splittings. It should be noted that although the general shapes of the $P(\Delta)$ distributions obtained using the shell model and the one-Gaussian-component model do not differ too much, the latter model fits the spectra much better. This shows that small changes in the shape of the $P(\Delta)$ distribution significantly influence the shapes of Mössbauer spectra. In other words, a careful analysis of Mössbauer spectra can provide the $P(\Delta)$ distributions which are very close to the true ones.

Table I. Parameters determined from the shell-model fits. $\bar{\delta}$ and $\bar{\Delta}$ designate the average values of δ and Δ. χ^2 is defined as $[\Sigma_{i=1}^{k}(y_i^{\text{expt}}-y_i^{\text{theor}})^2/y_i^{\text{expt}}]/(k\text{-}m)$, where k and m are, respectively, the number of experimental points and the number of fitted parameters. The parameters Γ, σ, $\bar{\Delta}$, δ_0, and $\bar{\delta}$ are in units of mm/s, and the unit of T is K. The values of δ are given relative to the source.

Sample	T	Γ	σ	n	$\bar{\Delta}$	δ_0	a	$\bar{\delta}$	χ^2
1	293	0.252(3)	0.321(4)	2.147(34)	0.419(1)	0.103(6)	−0.023(1)	0.093(1)	3.636
2	293	0.252(1)	0.305(1)	2.154(3)	0.399(1)	0.103(1)	−0.026(1)	0.093(1)	4.551
1	4.2	0.254(5)	0.347(7)	2.018(50)	0.436(1)	0.218(1)	−0.020(2)	0.210(1)	1.871
2	4.2	0.248(2)	0.325(3)	2.059(25)	0.414(1)	0.218(1)	−0.027(1)	0.207(1)	5.134

Table II. Parameters determined from the one-Gaussian-component-model fits. The meaning and the units of the symbols are the same as in Table I. The standard deviation σ_δ corresponding to the Gaussian distribution of δ is equal to $a\sigma_\Delta$.

Sample	T	Γ	σ_Δ	$\bar{\Delta}$	δ_0	a	$\bar{\delta}$	χ^2
1	293	0.245(1)	0.223(1)	0.406(1)	0.101(1)	−0.019(1)	0.093(1)	1.659
2	293	0.246(1)	0.212(2)	0.387(1)	0.102(1)	−0.022(1)	0.093(1)	1.912
1	4.2	0.244(1)	0.241(1)	0.421(1)	0.216(1)	−0.016(2)	0.210(1)	1.036
2	4.2	0.238(2)	0.228(2)	0.401(1)	0.216(1)	−0.022(1)	0.207(1)	1.473

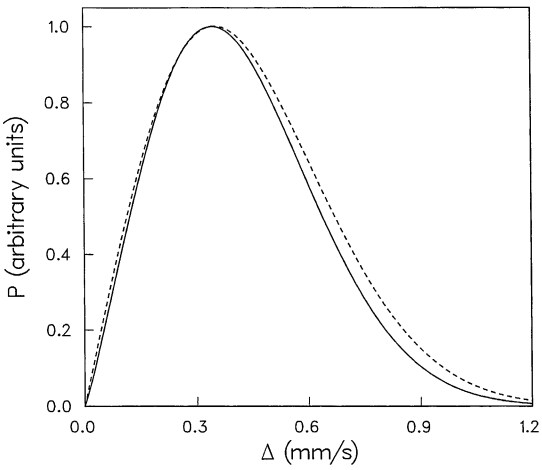

Fig. 5. Comparison of the shell-model distribution functions $P(\Delta)$ corresponding to the fits in Figs. 1(a) (solid line) and 3(a) (broken line).

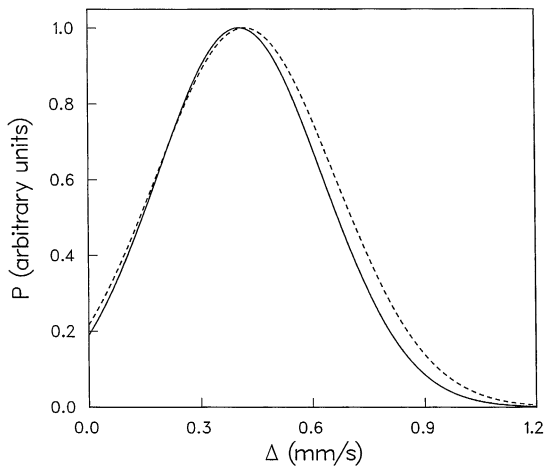

Fig. 6. Comparison of the one-Gaussian-component distribution functions $P(\Delta)$ corresponding to the fits in Figs. 1(b) (solid line) and 3(b) (broken line).

The shape of the $P(\Delta)$ distributions does not change significantly with temperature. Lowering the temperature leads to a slight broadening of the $P(\Delta)$ distribution, as can be clearly seen for both the shell-model and one-Gaussian-component-model distributions (Figs. 5 and 6). This is the consequence of the larger values of σ and σ_Δ parameters at 4.2 K as compared to the room-temperature values (Tables I and II). The average value $\bar{\Delta}$ decreases with temperature at the average rate of $-0.52\cdot10^{-4}$ mm/s/K, which is similar to the average rate of $-0.48\cdot10^{-4}$ mm/s/K found for the $Al_{65}Fe_{15}Cu_{20}$ icosahedral alloy.[13] The decrease of $\bar{\Delta}$ with temperature is caused by a complex, and as yet unknown, temperature dependence of the lattice and the valence-electron contributions to the EFG tensor.

The presence of a wide distribution of quadrupole splittings observed here and in other IA[9,10,13,27] is direct evidence for the existence of the multiplicity of Fe sites. This, in turn, shows that disorder must be an intrinsic characteristic of IA. Unfortunately, the lack of theoretical calculations of the distribution of the EFG in IA, which even for crystalline materials constitute a very complex and challenging theoretical endeavour, inhibits a comparison of the experimentally determined shapes of $P(\Delta)$ distributions with theory. Such calculations are very desirable since the experimentally determined shapes of $P(\Delta)$ could be directly used to determine which of the three structural models of IA mentioned before is the most appropriate.

The lack of a hyperfine magnetic dipole interaction in the 4.2 K Mössbauer spectrum of $Al_{70}Fe_{20}Ta_{10}$ (Fig. 3) proves that Fe atoms do not carry a magnetic moment. Thus, the $Al_{70}Fe_{20}Ta_{10}$ icosahedral alloy, similarly to another Fe-rich icosahedral alloy, $Al_{65}Fe_{25}Cu_{20}$,[13] is not magnetically ordered.

The distribution functions $P(\delta)$ obtained from the fits of the room-temperature and 4.2 K Mössbauer spectra using the one-Gaussian-component model are shown in Fig. 7. They have the same value of $\sigma_\Delta=0.004(1)$ mm/s and are centred respectively at $\bar{\delta}=0.093(1)$ mm/s and $\bar{\delta}=0.216(1)$ mm/s (Table II). The very small value of σ_Δ indicates that the disorder present in $Al_{70}Fe_{20}Ta_{10}$ has a very small effect on the values of the isomer shift. The average temperature change of $\bar{\delta}$ is $-4.26\cdot10^{-4}$ mm/s/K and is similar to the value of $-3.85\cdot10^{-4}$ mm/s/K found for the $Al_{65}Fe_{15}Cu_{20}$ icosahedral alloy.[13] This dependence is caused by the second-order Doppler effect.[20]

The fitted parameters of the Mössbauer spectra of sample 2, which contained a larger amount of second phases, do not differ substantially from the parameters of sample 1 (Tables I and II). The main difference is in the

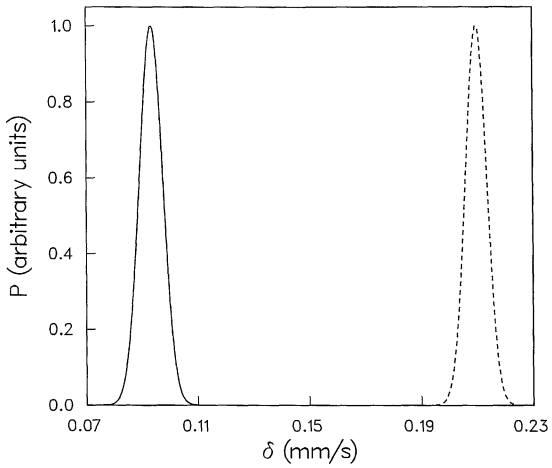

Fig. 7. The distribution functions $P(\delta)$ corresponding to the fits in Figs. 1(b) (solid line) and 3(b) (broken line).

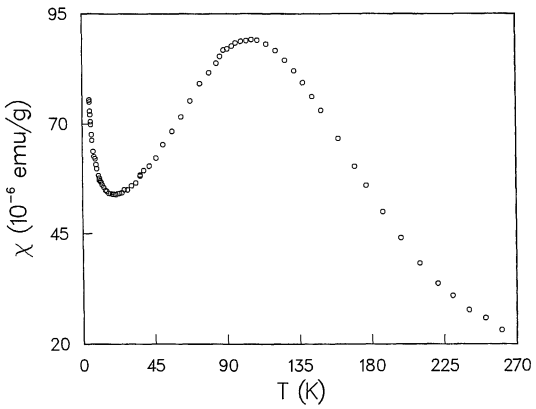

Fig. 8. Temperature dependence of zero-field cooled susceptibility of sample 1 measured in the field of 25.5 Oe.

value of $\bar{\Delta}$, which for sample 2 is a few per cent smaller than for sample 1. This can be explained by the fact that the Mössbauer spectrum[26] of Al_3Fe impurity artificially increases the values of $P(\Delta)$ for small Δ. As can be expected, the quality of the fits of the spectra of sample 2 is significantly worse in comparison to the fits of the spectra of sample 1 (Tables I and II).

3.3 Susceptibility data

The temperature dependence of the susceptibility of sample 1 is shown in Fig. 8. It exhibits a very broad cusp at 106 K. A very similar $\chi(T)$ dependence was found for sample 2. The broad cusp is not due to the icosahedral $Al_{70}Fe_{20}Ta_{10}$ but is the consequence of the presence of Al_3Fe, which is a paramagnet,[28] and possibly other minor magnetic second phases. The broad cusp is superimposed on a typical Curie-like $\chi(T)$ dependence, part of which can be seen at low temperatures (Fig. 8). It is well established that magnetic precipitates exhibit a cusp in the $\chi(T)$ dependence,[29] very similar to the cusp observed in spin glasses. The application of relatively small external magnetic fields results in the disappearance of this cusp.[29]

By comparing the $\chi(T)$ dependence in Fig. 8 with that shown in Fig. 5 of ref. 12 one can conclude that the non Curie-like behaviour of $\chi(T)$ measured in the field of 10 kOe,[12] which washed out the impurity cusp, is an artifact caused by the presence of magnetic second phases in the studied sample of $Al_{70}Fe_{20}Ta_{10}$. The sample studied by Srinivas *et al.*[12] must have had a similar amount of the second phases as sample 1 studied here since the values of $\chi(T)$ reported in ref. 12 are only slightly higher than the values found in this paper (Fig. 8). Thus the claim[12] of the simultaneous existence of Curie and Pauli paramagnetism in icosahedral $Al_{70}Fe_{20}Ta_{10}$ is highly questionable.

The low temperature (below 21 K) behaviour of the $\chi(T)$ dependence (Fig. 8) suggests that the $Al_{70}Fe_{20}Ta_{10}$ icosahedral alloy is probably a paramagnet. However, its magnetic parameters cannot be reliably determined until a truly single-phase sample can be produced.

§4. Summary

X-ray diffraction, ^{57}Fe Mössbauer spectroscopy and magnetic susceptibility measurements were performed in the temperature range 4.2–293 K on a new ternary icosahedral alloy $Al_{70}Fe_{20}Ta_{10}$. It was found that this alloy cannot be produced by a melt-spinning technique in a 100% single phase. The distributions of quadrupole splittings obtained from Mössbauer spectra reflected the intrinsic disorder present in icosahedral alloys. It was shown that this distribution is better described by the Gaussian shape than by the shape predicted by the shell model and that the

studied alloy is not magnetically ordered down to 4.2 K. Our results indicate that $Al_{70}Fe_{20}Ta_{10}$ is a paramagnet and the claim in the literature of the simultaneous existence of Curie-like and Pauli paramagnetism is an artifact resulting from the contribution to magnetic susceptibility of magnetic impurities present in the sample of $Al_{70}Fe_{20}Ta_{10}$.

Acknowledgment

This work was supported by the Natural Sciences and Engineering Research Council of Canada. We thank D. G. Rancourt and J. Y. Ping for making their multi-Gaussian-component computer program available to us.

References

1) D. Shechtman, I. Blech, D. Gratis and J. W. Cahn: Phys. Rev. Lett. **53** (1984) 1951.
2) *Aperiodicity and Order*, ed. M. V. Jarić and D. Gratis (Academic Press, Boston, 1989) Vol. 3; *Quasicrystals*, ed. T. Fujiwara and T. Ogawa (Springer-Verlag, Berlin, 1990).
3) K. M. Rabe, A. R. Kortan and J. C. Phillips: Phys. Rev. B**43** (1991) 6280.
4) C. Janot, M. De Boissieu, J. M. Dubois and J. Pannetier: J. Phys. Condens. Matter **1** (1989) 1029.
5) D. Levine and P. J. Steinhardt: Phys. Rev. B**34** (1986) 596.
6) D. Shechtman and I. A. Blech: Metall. Trans. A**16** (1985) 1005; P. W. Stephens and A. I. Goldman: Phys. Rev. Lett. **56** (1986) 1168.
7) M. Widom, D. P. Deng and C. L. Henley: Phys. Rev. Lett. **63** (1989) 310; K. J. Strandburg: Phys. Rev. B**40** (1989) 6071.
8) M. Rubinstein, G. H. Stauss, T. E. Phillips, K. Moorjani and L. H. Bennett: J. Mater. Res. **1** (1986) 243.
9) Z. M. Stadnik and G. Stroink: Phys. Rev. B**38** (1988) 10447.
10) Z. M. Stadnik and G. Stroink: Phys. Rev. B**43** (1991) 894.
11) A.-P. Tsai, A. Inoue and T. Masumoto: Jpn. J. Appl. Phys. **27** (1988) L5.
12) V. Srinivas, M. E. McHenry and R. A. Dunlap: Phys. Rev. B**40** (1989) 9590.
13) Z. M. Stadnik, G. Stroink, H. Ma and G. Williams: Phys. Rev. B**39** (1989) 9797, and references therein.
14) S. Matsuo, H. Nakano, T. Ishimasa and Y. Fukano: J. Phys. Condens. Matter **1** (1989) 6893; T. Klein, A. Gozlan, C. Berger, F. Cyrot-Lackmann, Y. Calvayrac, A. Quivy and G. Fillion: Physica B**165/166** (1990) 283.
15) D. G. Rancourt and J. Y. Ping: Nucl. Instrum. & Methods Phys. Res. B**58** (1991) 85.
16) Certificate of Calibration, Iron Foil Mössbauer Standard, Natl. Bur. Stand. (U.S.) Circ. No. 1541, ed. J. P. Cali (U.S. GPO, Washington, D.C., 1971).
17) G. Lamarche: Rev. Sci. Instrum. **60** (1989) 943.
18) A.-P. Tsai, A. Inoue and T. Masumoto: Jpn. J. Appl. Phys. **26** (1987) L1505.
19) V. Elser and Ch. L. Henley: Phys. Rev. Lett. **55** (1985) 2883; V. Elser: Phys. Rev. B**32** (1985) 4892.
20) N. N. Greenwood and T. C. Gibb: *Mossbauer Spectroscopy* (Chapman and Hall, London, 1971).
21) F. Varret, J. M. Grenche and J. Teillet: in *Trends in Mössbauer Spectroscopy, Proc. Second Seheim Workshop*, ed. P. Gutlich and G. M. Kalvius (University of Mainz, 1983) p. 105, and references therein; S. J. Campbell: *ibid.*, p. 117, and references therein.
22) M. Maurer, J. M. Friedt and J. P. Sanchez: J. Phys. F**15** (1985) 1449.
23) G. Czjzek, J. Fink, F. Götz, H. Schmidt, J. M. D. Coey, J.-P. Rebouillat and A. Liénard: Phys. Rev. B**23** (1981) 2513; G. Czjzek: Nucl. Instrum. & Methods **199** (1982) 37.
24) D. Bahadur, V. Srinivas and R. A. Dunlap: J. Phys. Condens. Matter **1** (1989) 2561.
25) J. Y. Ping, D. G. Rancourt and R. A. Dunlap: J. Magn. & Magn. Mater. (in press); J. Y. Ping, D. G. Rancourt and Z. M. Stadnik: Hyperfine Interact. (in press).
26) R. S. Preston and R. Gerlach: Phys. Rev. B**3** (1971) 1519; L. Murgás, S. Nagy, Z. Homonnay, A. Vértes and J. Lakner: Hyperfine Interact. **28** (1986) 967.
27) K. Edagawa, H. Ino, S. Nasu, K. Kimura, S. Takeuchi, T. Shinjo, K. Koga, T. Shimizu and H. Yasuoka: J. Phys. Soc. Jpn. **56** (1987) 2629; M. Eibschütz, M. E. Lines, H. S. Chen, J. V. Waszczak, G. Papaefthymiou and R. B. Frankel: Phys. Rev. Lett. **59** (1987) 2443.
28) G. Foèx and J. Wucher: C. R. Acad. Sci. (Paris) **238** (1954) 1281; G. Foex and J. Wucher: J. Phys. (Paris) **17** (1956) 454.
29) F. Söffge and W. Von Hörsten: Z. Phys. B**42** (1981) 47; D. Fiorani, J. L. Tholence and J. L. Dormann: J. Magn. & Magn. Mater. **31–34** (1983) 947.